Analysis and Measurement of 3D Torque and Forces for Permanent Magnet Motors with Slotless Windings

A. Looser, T. Baumgartner, C. Zwyssig and J.W. Kolar
Power Electronic Systems Laboratory
ETH Zurich
CH-8092 Zurich, Switzerland
looser@lem.ee.ethz.ch

***Abstract*—Slotless windings, skewed and rhombic, are widely used in industry. Beside the drive torque, possibly undesired transverse torques and forces are generated, which have not been analyzed previously. An analytical derivation of the torque and force components in all three directions is detailed in this paper for the skewed winding. It is shown that for some winding configurations alternating transverse torque components are generated, which may compromise stable operation in applications where for example magnetic or gas bearings are involved. Moreover the windings are analyzed with regard to a potential use as active magnetic radial bearings in high-speed applications. Finally, measurements are presented to verify the theoretical results.**

I. Introduction

Slotless windings are widely used for small sized electric motors in industrial applications ranging from a hundred milliwatts to a few hundred watts [1]. The main advantages of a slotless design are the absence of cogging torque, the elimination of losses caused by slot space harmonics, the low winding inductance. For the last two reasons it is also an excellent choice for high-speed motors [2].

An overview of different types of slotless windings is given in [3] and [4]. Commonly used winding types are the skewed type and the rhomic winding. As can be seen from Figure 1 both windings exhibit complex three dimensional structures with two layers overlapping. This can result in undesirable transverse torque and force components beside the intended drive torque in axial direction, even for perfect alignment and symmetry of the winding. In some high-speed applications where rotordynamics must be considered, e.g. when magnetic bearings or gas bearings are involved, these transverse torque components have to be either avoided by choosing an appropriate winding type, configuration and geometry or at least exactly quantified and incorporated into the rotordynamic model.

The magnetic field in the airgap required for the analysis of the torque and force components has been studied in [5], [6] and [7]. Winding factors for the harmonic field components resulting in alternating drive torque have been analyzed in [4]. However, no analysis or measurement of the transverse torque and forces components have been reported in literature.

(a) (b)

Fig. 1. Skewed winding (a) and rhombic winding (b)

In this paper torque and force calculations for the skewed type winding are derived. The most common configuration, the two-pole, three-phase winding is analyzed in detail, including possible force generation for an active magnetic bearing. A winding test bench is built and the theoretical results are verified by measurements.

II. Derivation of Force and Torque for the Skewed Winding

A. Magnetic Field Distribution

According to [5] the flux density in the airgap of a slotless permanent-magnet machine can be described by Fourier series for both the radial and the azimuthal field components as

$$B_r = \sum_{n=1}^{\infty} B_r^{(n)} \cos(nq\theta + \delta) \tag{1}$$

$$B_\theta = \sum_{n=1}^{\infty} B_\theta^{(n)} \sin(nq\theta + \delta), \tag{2}$$

where q is the number of pole pairs of the rotor, δ the load angle and $B_r^{(n)}$ and $B_\theta^{(n)}$ are the Fourier coefficients of the n^{th} harmonic. The field in axial direction is assumed to be $B_z = 0$.

It is well known that for machines driven with symmetric sinusoidal currents only the fundamental component contributes to a constant torque. Therefore, from a design point of view,

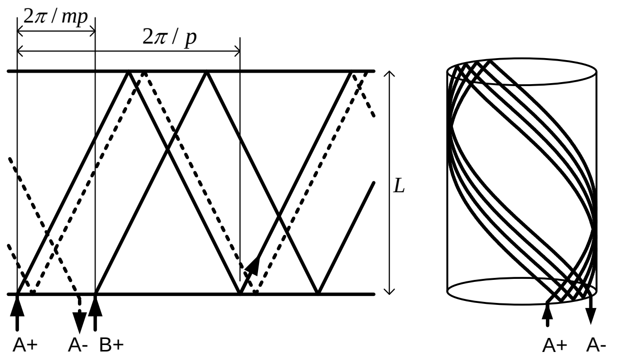

Fig. 2. Winding scheme and 3D structure of the skewed type winding.

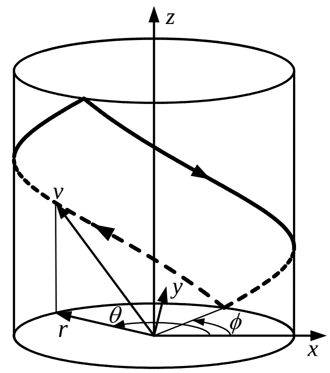

Fig. 3. Coordinate system definition and winding loop parametrization.

the flux density of an optimal machine only consists of the fundamental component, and hence for the winding analysis carried out in this paper it is assumed that that the geometry of the rotor and the permanent-magnets is chosen such that all the harmonic field components vanish. Indeed for the $q = 1$ pole pair machine a purely fundamental field distribution is achieved by a diametral magnetization direction in the cylindrical permanent-magnet [7].

The time varying fundamental field in the airgap for a rotor rotating with speed Ω is then described in cylindrical coordinates by

$$B_r = \hat{B}_r(r) \cdot \cos(q\theta - q\Omega t + \delta) \tag{3}$$

$$B_\theta = \hat{B}_\theta(r) \cdot \sin(q\theta - q\Omega t + \delta) \tag{4}$$

To derive the force and torque components in cartesian coordinates is described by

$$\boldsymbol{B} = \begin{bmatrix} B_r \cdot \cos(\theta) - B_\theta \cdot \sin(\theta) \\ B_r \cdot \sin(\theta) + B_\theta \cdot \cos(\theta) \\ 0 \end{bmatrix}. \tag{5}$$

B. Winding Definition

A winding is defined by the number of phases $m \geq 3$ and the number of pole pairs p. It is to be noted that the pole pair number of the rotor q does not necessarily need to be equal to pole pair number of the winding p. For each pole a winding zone spreads over an angle $\varphi/p = 2\pi/mp$ with $\varphi = 2\pi/m$ being the electrical phase shift from one phase to the adjacent phase (Figure 2).

For $m = 1$ and $m = 2$ a different winding descriptions would be necessary. However, because no constant torque can be achieved with a one-phase winding, it is not considered further. The two-phase winding has a very low utilization factor when having only two windings situated $\pi/2$ to each other, because then only half of the volume is used for the winding. However introducing windings connected in series on the opposite sides in the unused space to overcome this drawback results then in an $m = 4$ phase winding, which is then covered by the given definition.

A single winding loop starting from angle ϕ as depicted in Figure 3 can be described by the vector

$$\boldsymbol{v} = \begin{bmatrix} r \cdot \cos(\theta) \\ r \cdot \sin(\theta) \\ z(\theta) \end{bmatrix} \tag{6}$$

with the z component given by

$$z(\theta) = -\frac{L}{2} + \frac{pL}{\pi} \cdot \begin{cases} (\theta - \phi), & \text{for} \quad 0 < \theta - \phi < \frac{\pi}{p} \\ (\frac{2\pi}{p} - \theta + \phi), & \text{for} \quad \frac{\pi}{p} < \theta - \phi < \frac{2\pi}{p} \end{cases} \tag{7}$$

and L being the winding hight in z direction.

The current density in the winding loop belonging to a phase conducting a current of phase shift φ is given by

$$\boldsymbol{J} = J \frac{d\boldsymbol{s}}{\|d\boldsymbol{s}\|} \tag{8}$$

where J is defined as

$$J = \hat{J} \cdot \cos(q\Omega t - \varphi) \tag{9}$$

and $d\mathbf{s}$ is given by

$$d\mathbf{s} = \frac{\partial \boldsymbol{v}}{\partial \theta} d\theta. \tag{10}$$

C. 3D Force and Torque

The Lorentz force on a infinitesimal conductor element with volume dV calculated from the triple product

$$dV = |(r d\boldsymbol{\phi} \times d\boldsymbol{r}) \cdot d\mathbf{s}| = \frac{pL}{\pi} d\theta r d\phi dr \tag{11}$$

is given by

$$d\boldsymbol{F} = \frac{1}{2} \boldsymbol{J} \times \boldsymbol{B} \cdot dV = \frac{J \cdot \frac{\partial \boldsymbol{v}}{\partial \theta} \times \boldsymbol{B}}{2\sqrt{1 + \left(\frac{\pi r}{pL}\right)^2}} d\theta r d\phi dr \tag{12}$$

where the factor $\frac{1}{2}$ results from the two layer structure of the winding. The torque generated by that element in respect to the origin is given by

$$d\boldsymbol{T} = \boldsymbol{v} \times d\boldsymbol{F}. \tag{13}$$

The torque and the force generated by a single phase is then obtained by integration over one winding loop and one phase zone and summation over all pole pairs as

$$\boldsymbol{T}_{ph} = J\sum_{k=0}^{p-1}\int_{R_3}^{R_4}\int_{\frac{\varphi+2\pi k-\pi/m}{p}}^{\frac{\varphi+2\pi k+\pi/m}{p}}\int_{\phi}^{\phi+\frac{2\pi}{p}} \frac{\boldsymbol{v}\times\frac{\partial \boldsymbol{v}}{\partial\theta}\times\boldsymbol{B}}{2\sqrt{1+\left(\frac{\pi r}{pL}\right)^2}} d\theta r d\phi dr \tag{14}$$

and

$$\boldsymbol{F}_{ph} = J\sum_{k=0}^{p-1}\int_{R_3}^{R_4}\int_{\frac{\varphi+2\pi k-\pi/m}{p}}^{\frac{\varphi+2\pi k+\pi/m}{p}}\int_{\phi}^{\phi+\frac{2\pi}{p}} \frac{\frac{\partial \boldsymbol{v}}{\partial\theta}\times\boldsymbol{B}}{2\sqrt{1+\left(\frac{\pi r}{pL}\right)^2}} d\theta r d\phi dr, \tag{15}$$

where R_3 and R_4 are the winding inner and the winding outer radius (see Figure 4). Summing up over all m phases yields the total torque and the total force

$$\boldsymbol{T} = \sum_{k=0}^{m-1} \boldsymbol{T}_{ph}\Big|_{\varphi=\frac{2\pi k}{m}} \tag{16}$$

and

$$\boldsymbol{F} = \sum_{k=0}^{m-1} \boldsymbol{F}_{ph}\Big|_{\varphi=\frac{2\pi k}{m}}. \tag{17}$$

D. Solution for $p = q$

Evaluating (14) and (16) yields the the torque

$$\boldsymbol{T} = \begin{bmatrix} T_x \\ T_y \\ \frac{-4m\sin(\frac{\pi}{m})\hat{J}L\sin(\delta)}{\pi}\int_{R_3}^{R_4}\frac{\hat{B}_r r^2 dr}{\sqrt{1+\left(\frac{\pi r}{pL}\right)^2}} \end{bmatrix} \tag{18}$$

where for $p = 1$ and $m = 3$ the transverse torque components are

$$T_x = \frac{3\sqrt{3}\hat{J}L^2\sin(2\Omega t-\delta)}{8\pi}\int_{R_3}^{R_4}\frac{\left(\hat{B}_r+\hat{B}_\theta\right) r dr}{\sqrt{1+\left(\frac{\pi r}{pL}\right)^2}} \tag{19}$$

and

$$T_y = \frac{3\sqrt{3}\hat{J}L^2\cos(2\Omega t-\delta)}{8\pi}\int_{R_3}^{R_4}\frac{\left(\hat{B}_r+\hat{B}_\theta\right) r dr}{\sqrt{1+\left(\frac{\pi r}{pL}\right)^2}}. \tag{20}$$

For any other combination of m and $p > 1$ the transverse torque components vanish ($T_x = T_y = 0$).

Evaluating (15) and (17) yields a vanishing force $\boldsymbol{F} = \boldsymbol{0}$ for any combination of p and m.

E. Two-Pole Three-Phase Winding

For the two-pole three-phase winding , $q = p = 1$, $m = 3$ the transverse torque components T_x and T_y given by (19) and (20) do not vanish but alternate with a frequency of twice the rotational speed. In order to compare the amplitudes of the drive torque T_z and the transverse torque components T_x and T_y the integral over the radius needs to be solved and therefore the radial dependency of the flux density has to be considered.

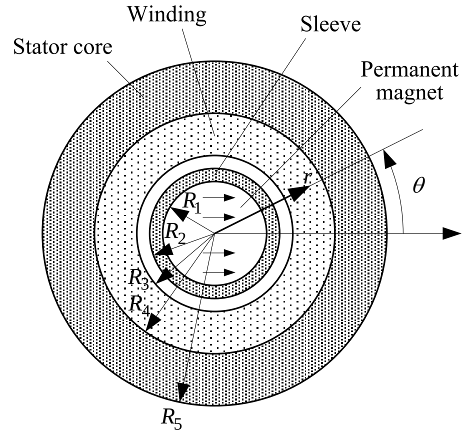

Fig. 4. Machine cross-section and symbol definitions: diametrically magnetized cylindrical permanent-magnet rotor inside a slotless stator [7].

The equations for the flux density $\boldsymbol{B}$ for $q = 1$ are derived in [7] and the parameter definitions are given in Figure 4. Simplifying the equations for the radial and azimuthal components of the flux density by setting the relative permeability of the permanent-magnet and the stator back iron $\mu_{r,pm} \approx 1$ respectively $\mu_{r,Fe} \to \infty$ yields

$$\hat{B}_r(r) = \frac{B_{rem}R_1^2}{2R_4^2}\left(\frac{R_4^2}{r^2}+1\right) \tag{21}$$

$$\hat{B}_\theta(r) = \frac{B_{rem}R_1^2}{2R_4^2}\left(\frac{R_4^2}{r^2}-1\right). \tag{22}$$

The torque generated by a $m = 3$ phase winding is obtained by evaluating (18), (19) and (20) to

$$\boldsymbol{T} = \begin{bmatrix} \frac{3\sqrt{3}\hat{J}B_{rem}L^2R_1^2\sin(2\Omega t-\delta)}{32\pi}\cdot K_1 \\ \frac{3\sqrt{3}\hat{J}B_{rem}L^2R_1^2\cos(2\Omega t-\delta)}{32\pi}\cdot K_1 \\ \frac{-3\sqrt{3}\hat{J}B_{rem}L^2R_1^2\sin(\delta)}{4\pi^4}\cdot K_2 \end{bmatrix} \tag{23}$$

where the K_1 and K_2 are given by

$$K_1 = log\left(\frac{L+\sqrt{L^2+\pi^2R_3^2}}{L+\sqrt{L^2+\pi^2R_4^2}}\cdot\frac{L-\sqrt{L^2+\pi^2R_4^2}}{L-\sqrt{L^2+\pi^2R_3^2}}\right) \tag{24}$$

and

$$K_2 = \frac{1}{R_4^2}\Bigg[\pi R_4\sqrt{L^2+\pi^2R_4^2} - \pi R_3\sqrt{L^2+\pi^2R_3^2} + (2\pi^2R_4^2-L^2)\cdot log\left(\frac{\pi R_4+\sqrt{L^2+\pi^2R_4^2}}{\pi R_3+\sqrt{L^2+\pi^2R_3^2}}\right)\Bigg]. \tag{25}$$

A high ratio of L/R_4 and R_3/R_4 results in windings producing relatively high transverse torque T_{xy} compared to the drive torque T_z as can be seen from Figure 5. This is rather unfavorable since for common machines the winding length is usually larger than its outer diameter leading to a

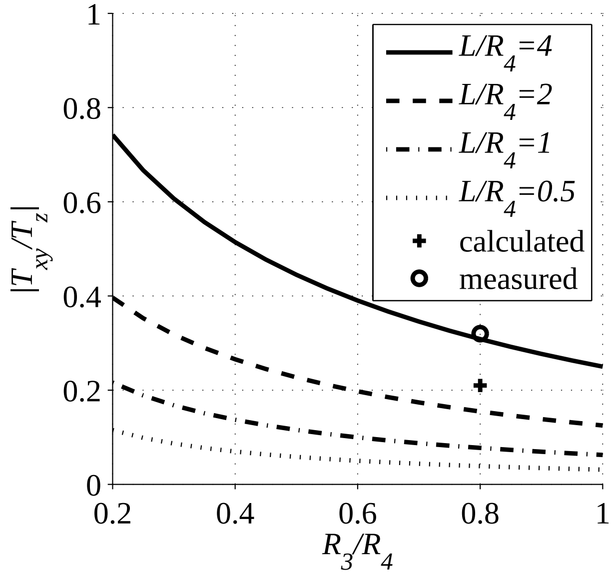

Fig. 5. Ratio of transverse torque T_{xy} to drive torque T_z for the two-pole, three-phase winding in dependency of the geometry parameters active length L, winding inner radius R_3 and winding outer radius R_4. The calculated value for the experimental winding of Table I is shown with a cross, the measured value with a circle.

the transverse torque in the area of 10% to 20% of the drive torque or more.

III. Force Generation for Active Magnetic Bearings

The skewed type winding is a promising candidate for an active magnetic bearing for high-speed applications due to its low inductance and the relatively low negative stiffness resulting from the large magnetic air gap [8]. There are many configurations for generating a net force; e.g. for the configuration $p = q + 1$ the torque always vanishes: $\boldsymbol{T} = \mathbf{0}$. The force for this configuration and $m \geq 3$ is obtained from (15) and (17) as

$$\boldsymbol{F} = -\frac{2mJL\sin\left(\frac{\pi}{m}\right)}{\pi} \int_{R_3}^{R_4} \frac{\left(\hat{B}_r + \hat{B}_\theta\right) rdr}{\sqrt{1+\left(\frac{\pi r}{pL}\right)^2}} \begin{bmatrix} cos(\delta) \\ sin(\delta) \\ 0 \end{bmatrix}. \quad (26)$$

For $q = 1$ the simplifications for the flux density $\boldsymbol{B}$ made in section II-E can be used to calculate the integral in (26) yielding

$$\boldsymbol{F} = -\frac{m\sin(\frac{\pi}{m})K_3 JLR_1^2 B_{rem}}{\pi} \begin{bmatrix} cos(\delta) \\ sin(\delta) \\ 0 \end{bmatrix} \quad (27)$$

where K_3 is defined as

$$K_3 = log\left(\frac{2L+\sqrt{4L^2+\pi^2R_3^2}}{2L+\sqrt{4L^2+\pi^2R_4^2}} \cdot \frac{2L-\sqrt{4L^2+\pi^2R_4^2}}{2L-\sqrt{4L^2+\pi^2R_3^2}}\right). \quad (28)$$

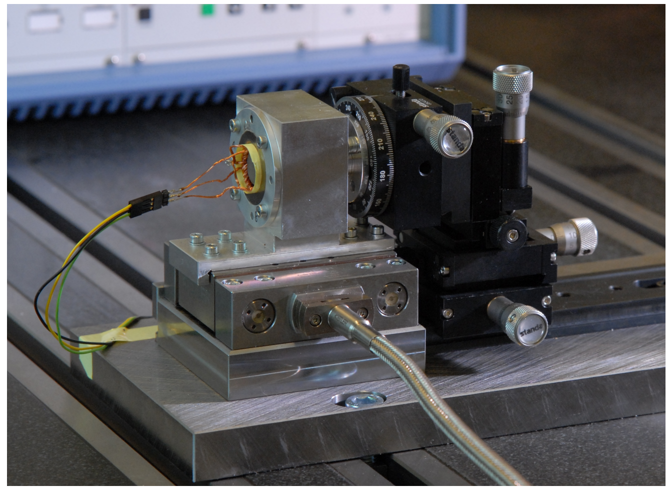

Fig. 6. Winding test bench with the stator mounted on the piezoelectric load cell and the permanent-magnet fixed to the positioning stage.

IV. Measurements

A. Measurement Setup

The measurements are performed on a granite measurement platform. The permanent-magnet is mounted on a xyz-translation stage with an additional rotational stage allowing for accurate positioning and rotation of the magnet. The stator is mounted on a multi component load cell to measure the winding reaction force and torque components resulting from the injected winding currents. A photograph of the described assembly is shown in Figure 6.

A Spitzenberger&Spies DM3000 power supply is used to generate the three-phase symmetric sinusoidal currents fed to the star configured winding at a frequency of 1 Hz. The three phase currents are measured with current sensors (LEM LTS 6-NP). The current sensor output signals and force signals are acquired by a National Instruments LabVIEW card at a sample rate of 1 kHz.

The motor winding to be measured is expected to deliver a nominal drive torque of 30 mNm. In order to measure such small quantities a piezoelectric multi component dynamometer (Kistler 9256C1) is used, providing six force measurements in pairs F_{x1} and F_{x2}, F_{y1} and F_{y2} and F_{z1} and F_{z2}, and thereby allowing to compute the resulting forces as well as two of the three torque components. The force components are $F_x = F_{x1} + F_{x2}$, $F_y = F_{y1} + F_{y2}$ and $F_z = F_{z1} + F_{z2}$ and the two torque components are $T_y = a\cdot(F_{x1} - F_{x2}) + b\cdot(F_{z1} - F_{z2})$ and $T_z = c \cdot (F_{y1} - F_{y2}) + d \cdot F_x$, where the term $d \cdot F_x$ accounts for the coordinate transformation from the sensor to the stator coordinate system $(x, y, z) \to (x, y + d, z)$. a, b and c result from the load cell geometry. To obtain the torque T_x the measurements are repeated for the winding rotated by an angle of $90°$.

A multichannel charge amplifier from Kistler of type 5017 is used. For all the measurements the amplifier's internal second order low-pass filters are used and the cut-off frequency is set to 300 Hz.

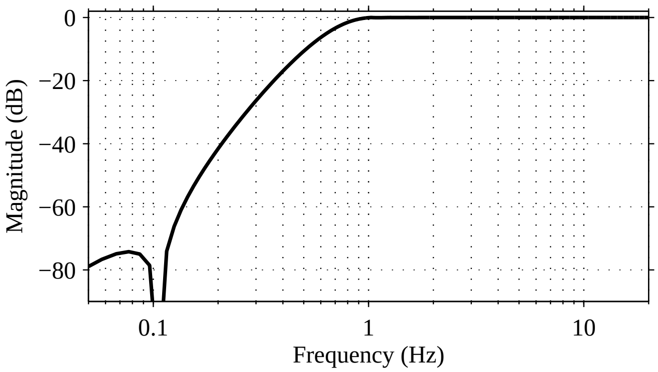

Fig. 7. Frequency response of the drift compensation FIR filter with an attenuation of 0.056 dB at 1.0 Hz.

To verify correct behavior of the load cell, quasi-static measurements of test forces applied by a dial gauge and test weights were carried out. It was concluded that the resulting forces and the torque T_y was measured with high precision, while for T_z the measured values were 32% lower. Therefore a correction factor had to be introduced for the calculation of T_z.

As the generated charge produced by the small forces is low and the charge amplifier operates with high gain, signal drifting needs to be compensated. It is common for piezoelectric force measurements, that drift compensation is done manually by subtracting a linear approximation of the drift considering the beginning and the end of the measurement when no forces are applied. For symmetric sinusoidal three phase currents the resulting force and torque components are supposed to be offset-free. This simplifies drift compensation and the measured data can be processed off-line through a FIR high-pass filter and therewith eliminating the frequency components below 1 Hz. The frequency response of the applied drift compensation filter is shown in Figure 7.

B. Two-Pole Three-Phase Winding

The geometric data for the $q = p = 1$ test motor is listed in Table I. Sinusoidal three phase currents are injected such that the resulting stator field rotates in mathematically positive direction. Figure 8 shows the measured force and torque components for the rotor position $\theta = 0$ after signal drift compensation. Note that for the rotor fixed at position $\theta = 0$ and the stator field rotating in positive direction the load angle is $\delta = \Omega t$. Measurements are repeated for rotor positions in steps of 10°. Another series of measurements is furthermore required to obtain the torque component M_x by turning the winding by 90°. Figure 9 shows the combined resulting force and torque components from these measurements for a load angle $\delta = -\pi/2$, where the maximum drive torque is generated. It can be seen that the transverse torque rotates with twice the rotational speed. For the tested winding the ratio of transverse torque to drive torque is expected to be $T_{xy}/T_z = 0.21$, however the measurement shows a different ratio with 0.32, see Figure 5. Also the force components do

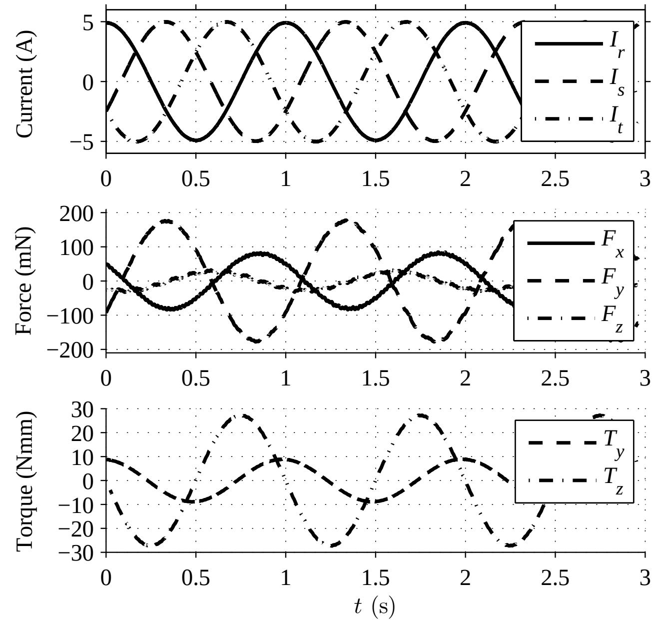

Fig. 8. Measurement of stator reaction torque and forces for the one pole pair three-phase test motor with injected stator currents at rotor position $\theta = 0$.

TABLE I
TWO-POLE THREE-PHASE TEST MOTOR

Symbol	Quantity	Value
R_1	Permanent-magnet radius	7.1 mm
R_3	Winding inner radius	8.0 mm
R_4	Winding outer radius	10.0 mm
R_5	Iron outer radius	15.0 mm
L	Active length	27.5 mm
B_r	Remanent flux density	1.1 T
N	Turn number per Winding	24

not vanish completely. These non-vanishing forces are up to 20% of the torque producing differential forces in the sensor. It can be excluded that these discrepancies result from not perfectly symmetric currents, as the current measurement error is smaller than 1% and the amplitude deviation of the injected currents was less than 1%. The errors however may be caused by misalignment of rotor and stator. The centering of the rotor in the axial direction is satisfactorily achieved by minimizing the resulting force in z-direction. However the resulting forces in x- and y-directions are very sensitive to the positioning of the rotor in these directions. Moreover, minimizing the forces for a specific angular rotor position did not yield satisfying results for other angular rotor positions. Another source for the non-vanishing forces might be the two layer structure and therewith associated asymmetries of the winding which has not been accounted for in the above modeling.

C. Active Magnetic Bearing Winding

Measurements have also been performed for a slotless type active magnetic bearing winding with a $p = 2$ pole pair skewed winding and a $q = 1$ pole pair rotor. The geometry is chosen the same as for the one pole pair test motor (Table I), except for the winding pole pair number. The measurement procedure

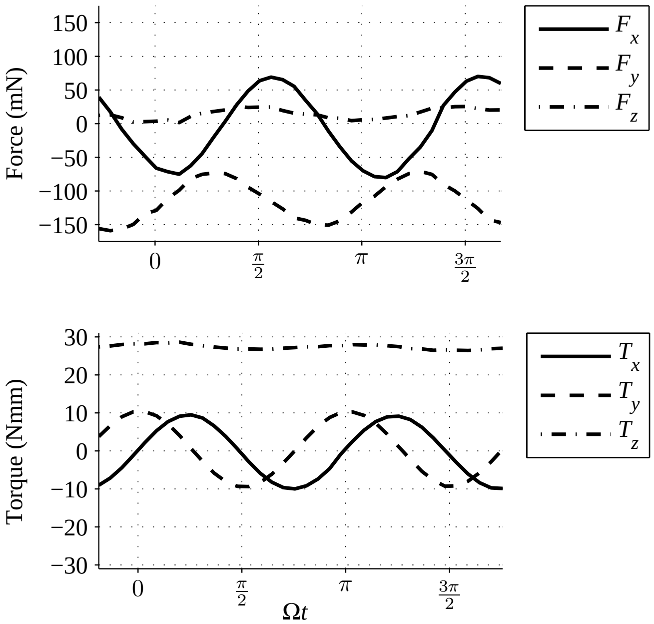

Fig. 9. Combined measured torque and forces for the one pole pair three-phase test motor for a constant load angle of $\delta = -\pi/2$.

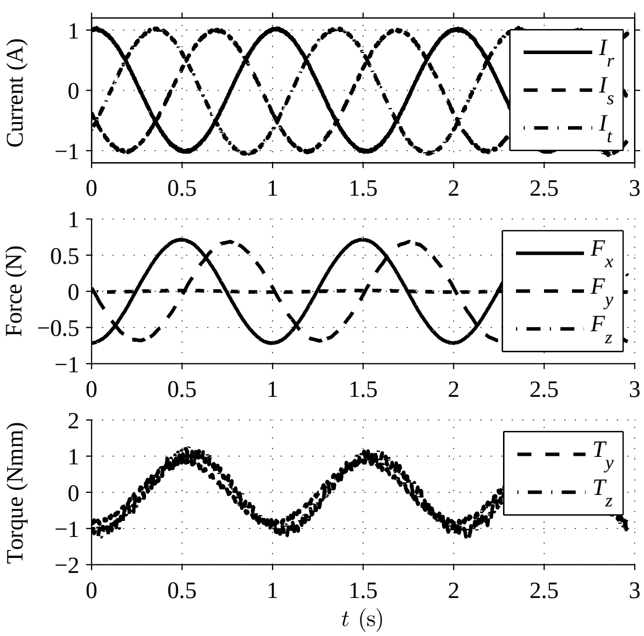

Fig. 10. Measurement of stator reaction torque and forces for the slotless magnetic bearing at $\theta = 0$.

is also exactly the same. However the phase currents needed to be set much lower not to overdrive the charge amplifier, which configuration was not changed. Figure 10 shows the measurement for a fixed rotor position at $\theta = 0$ while the three phase currents are applied. It can be seen that forces can be generated in both x- and y-direction with generating only very small amount of undesired torque or an axial force. Also, thecalculated force amplitude values are in very good agreement with the measured values. The calculated force amplitude for a peak current of 1 A resulting in a current density of $\hat{J} = 1.43\ \mathrm{A/mm^2}$ is 0.72 N, while the measured value range is 0.69 N to 0.71 N.

V. Conclusion

The skewed type winding with three phases and one pole pair $q = p = 1$ is widely used in industrial motor applications. Despite its popularity, its peculiarity to produce transverse torque components in addition to the drive torque seems not to be well known. However when rotor dynamics are of concern, e.g. when magnetic or gas bearings are involved, a thorough evaluation of the winding behavior is crucial. Therefore analytical expressions for the 3D force and torque are presented in this paper. For the two-pole winding, the measurements verify the existence of transverse torques with twice the frequency of the rotational speed, however with even a higher transverse to axial torque ratio than calculated. For the magnetic bearing winding the theoretical results are in very good agreement with the measurements. This proves the feasibility of using such a winding for a magnetic bearing.

Acknowledgments

The authors would like to thank Josef Stirnimann and Jens Boos from inspire AG for kindly providing the piezoelectric load cell and technical advice. A special thanks goes to Mark Vohrer from ATE GmbH for manufacturing the test windings.

References

[1] U. Kafader and J. Schulze, "Similarity relations in electromagnetic motors - limitations and consequences for the design of small dc motors," in *Proceedings of 9th International Conference on New Actuators (ACTUATOR '04)*, 2004, pp. 309–312.

[2] N. Bianchi, S. Bolognani, and F. Luise, "Potentials and limits of high-speed PM motors," vol. 40, no. 6, pp. 1570–1578, Nov.–Dec. 2004.

[3] M. Nagrial, J. Rizk, and A. Hellany, "Design and performance of permanent magnet slotless machines," in *Electrical Machines, 2008. ICEM 2008. 18th International Conference on*, Sept. 2008, pp. 1–5.

[4] B. Hagemann, "Entwicklung von Permanentmagnet-Mikromotoren mit Luftspaltwicklung," Ph.D. dissertation, Universitt Hannover, Germany, 1998.

[5] K. Sridhar, "Electromagnetic models for slotless pm synchronous motor drives," in *Applied Power Electronics Conference and Exposition, 1995. APEC '95. Conference Proceedings 1995., Tenth Annual*, no. 0, Mar 1995, pp. 367–377 vol.1.

[6] M. Markovic and Y. Perriard, "Simplified design methodology for a slotless brushless dc motor," *Magnetics, IEEE Transactions on*, vol. 42, no. 12, pp. 3842–3846, Dec. 2006.

[7] J. Luomi, C. Zwyssig, A. Looser, and J. W. Kolar, "Efficiency optimization of a 100-W, 500 000-rpm permanent-magnet machine including air friction losses," in *Proceedings of IEEE 42nd IAS Annual Meeting Industry Applications Conference (IAS '07)*, 2007, pp. 861–868.

[8] T. Baumgartner, A. Looser, C. Zwyssig, and J. W. Kolar, "Novel high-speed, lorentz-type, slotless self-bearing motor," to be published.